Impact of spatial resolution on large-scale ice cover modelling of mountainous regions

Helen Werner[1, 2], Dirk Scherler[1, 3], Tancrède P. M. Leger[4], Guillaume Jouvet[4], Ricarda Winkelmann[2, 5, 6]

[1]Organic and Earth Surface Geochemistry, GFZ Helmholtz Centre for Geosciences, 14473 Potsdam, Germany
[2]Earth Resilience Science Unit, PIK Potsdam Institute for Climate Impact Research, 14473 Potsdam, Germany
[3]Institute of Geographical Sciences, Freie Universität Berlin, 12249 Berlin, Germany
[4]IDYST, Faculty of Geosciences and Environment, Université de Lausanne, CH-1015 Lausanne, Switzerland
[5]Institute of Physics and Astronomy, University of Potsdam, 14476 Potsdam, Germany
[6]Department of Integrative Earth System Science, Max Planck Institute of Geoanthropology, 07745 Jena, Germany

Correspondence to: Helen Werner (helen.werner@gfz.de)

Abstract. To compensate for the high computational costs when modelling large-scale mountain glaciers, ice fields or ice sheets over multiple millennia, it is common practice to coarsen the spatial resolution of numerical models to 1 km or more, which is not sufficient to describe complex valley topographies. Here, we examine the influence of spatial resolution by modelling a growing and retreating ice field at resolutions ranging from 50 m to 2 km using the Instructed Glacier Model (IGM). We find that while ice-covered areas remain similar, ice volume increases substantially with coarser resolution. Compared to the reference run at 50 m spatial resolution, model results at a resolution of 300 m and finer are comparable and sufficiently accurate to simulate topographically constrained ice flow. However, at resolutions coarser than ~800 m, topographic resampling artificially lowers slope angles and mountain peaks, providing a larger accumulation area at high altitudes, with thicker glaciers that are typically warm-based, while thinner glaciers at fine resolutions remain cold-based. Raised valley floors at coarse resolutions result in slower-flowing ice with increased thickness and glacial response times. When the rate of temperature forcing is reduced by half, the hysteresis between climate forcing and glacial response at coarse resolutions is partially decreased, but the impact on other resolution effects is limited. Seemingly stable model results at coarse resolutions may be misleading and accurate glacier geometries might arise from parameter choices that compensate for poorly resolved topography. Non-linear and altitudinal-dependent resolution effects are likely in mountain regions worldwide and emphasize the need for model advances to enable simulations at sufficiently high spatial resolutions to accurately resolve glacier dynamics.

1 Introduction

Mountain glaciers are a crucial component of the Earth's cryosphere, providing freshwater to approximately 1.9 billion people (Immerzeel et al., 2020). Anthropogenic climate change threatens these resources and simultaneously increases the risk of natural hazards in mountainous regions, such as ice-rock avalanches and glacier lake outburst floods (Hartmeyer et al., 2020; Huggel et al., 2019). On a global scale, glacier melt contributed to about 20 % of sea-level rise between 2000 and 2019 (Hugonnet et al., 2021). Over longer time scales, glaciers play an important role in shaping the landscape of many mountain ranges. In the European Alps, extensive glaciations carved steep and narrow peaks and formed over-deepened and U-shaped valleys during the Quaternary period (Ivy-Ochs, 2015; Liebl et al., 2021; Penck and Brückner, 1909). Studying past glaciations helps us to understand the future evolution of mountain glaciers under present-day climate change. Consequently, spatially distributed and accurate numerical models of mountain glaciers and ice fields are essential for both projecting future change and reconstructing former glaciations.

The horizontal resolution of numerical ice models has been shown to influence simulations of continental-scale ice sheet mass loss and estimated sea-level contributions, particularly in regions with high bedrock elevation gradients (Cuzzone et al., 2019; Rückamp et al., 2020; Williams et al., 2025; Aschwanden et al., 2016). In order to address resolution-related model inaccuracies, Williams et al. (2025) suggest resolutions of 5 km or finer for modelling regions in the West-Antarctic ice sheet. For Greenland, Cuzzone et al.

(2019) propose a resolution of at least 10 km, Rückamp et al. (2020) report convergence of ISMIP6 (Ice Sheet Model Intercomparison Project; Nowicki et al., 2016) simulations at 1 km or finer, and Aschwanden et al. (2016) finds that a resolution of ~600 m is required to model most Greenland outlet glaciers in agreement with observational data. Resolution-related issues in ice sheet simulations may be efficiently mitigated using unstructured grids that refine the resolution in steep areas while keeping regions of more gentle sloping bedrock coarser (Cuzzone et al., 2019). However, for numerical models of mountain glaciers and ice fields, which are substantially controlled by the bedrock topography, resolution effects are expected to be stronger. Previous modelling studies of mountain-range scale glacier systems and ice fields in, e.g., the European Alps, the Tibetan Plateau, the Southern Alps of Zealand, typically used a km-scale resolution (e.g., Mey et al., 2016; Seguinot et al., 2018; Jouvet et al., 2023; Golledge et al., 2012; Zhang et al., 2022), but a systematic analysis of the impact of grid resolution is lacking.

Alpine regions are characterized by a complex topography with high mountain peaks and narrow valleys connected by steep slopes. These topographical features influence the formation, dynamics, and mass balance of glaciers. For example, surface elevation controls the mass balance mainly through the temperature lapse-rate, whereas the steepness of the bed controls glacier flow. However, when resampling a digital elevation model (DEM) to a coarser resolution, some of the topographical details for peaks and valleys are lost due to spatial averaging (Fig. 1d, e). For example, with 4806 m a.s.l., the Mont Blanc, the highest peak of the European Alps, attains a height of 4745 m in a 100 m DEM, and only 4674 m when resampled to 1 km resolution. This leads to an overall loss of area at high altitudes in coarser-resolution DEMs (Fig. 1b). Similarly, steep slopes in high-relief mountain regions of typically 30 ° and more (e.g., Duncan et al., 2003; Korup et al., 2005) are reduced by resampling DEMs to coarser resolution, thereby changing first-order topographical characteristics. Specifically, at elevations higher than 1000 m a.s.l. in the Western Alps, average slope angles in a 100 m DEM are ~5–10 ° steeper compared to a 500 m DEM and even ~10–15 ° steeper compared to a 1000 m DEM (Fig. 1c). Coarse resolutions therefore fail to accurately represent the mountain topography that controls glacier dynamics.

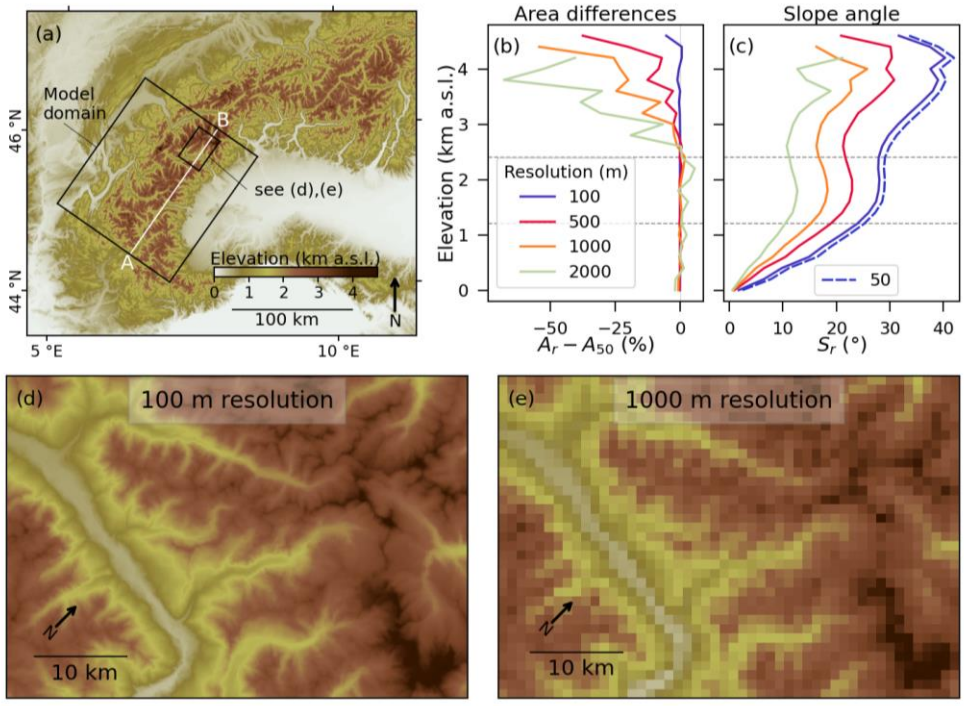

Figure 1 Comparison of a digital elevation model (DEM) at different resolutions. (a) DEM of the Western Alps at 300 m resolution (cubically resampled from a 30 m resolution DEM from Tadono et al. [2014] with present-day glaciers and lakes removed using data from Cook et al., [2023]). Large rectangle indicates the model domain; small rectangle indicates subsets shown in (d) and (e). White line indicates transect between points A and B shown in Fig. 6. (b) Area differences between DEMs at different resolutions *r* (A_r) and 50 m (A_{50}) relative to the 50 m DEM as a function of elevation. Area corresponds to the Western Alps shown in (a) and differences are averaged in 200 m elevation bins defined by the 50 m DEM. (c) Slope angles of the Western Alps shown in (a) at different resolutions *r*, averaged in 200 m elevation bins defined by 50 m DEM.

Resolutions shown in (b) and (c) are 100 (blue), 500 (red), 1000 (orange), and 2000 m (grey); and 50 m in (c) (blue dashed). Dashed grey horizontal lines (b) and (c) at 1200 and 2400 m a.s.l. mark our defined thresholds for low (0–1200 m a.s.l.), mid (1200–2400 m a.s.l.), and high altitudes (<2400 m a.s.l.). DEMs of small rectangle subset shown in (a) at (d) 100 m and (e) at 1 km resolution.

To improve numerical models, they are calibrated with geological data, such as mapped and dated moraines or trimlines (e.g., Kamleitner et al., 2022; Wirsig et al., 2016; Mey et al., 2016). In the European Alps, comparisons between modelled ice surface elevations and trimlines suggests ice thickness overestimations during the Last Glacial Maximum (LGM, ~24,000 years ago) in models based on a km-scale resolution, e.g., by up to 1000 m in the Rhône Valley (Seguinot et al., 2018; Jouvet et al., 2023). A better match between modelled ice surface elevations and trimlines at the same resolution was achieved by Mey et al. (2016) by adjusting the sliding coefficient. Recent work by Leger et al. (2025) significantly reduced the mean mismatch to ~150 m by using a higher spatial resolution of 300 m in an ensemble of 100 simulations with various parameter combinations. These results suggest that the agreement between numerical models and field data can be reduced not only through improved parameter choices but also by increasing the spatial resolution. However, it remains unclear whether even finer resolutions lead to more accurate results, and how spatial resolution influences other aspects of glacier modelling in alpine regions.

In this study, we explore the impact of spatial resolution on large-scale ice-cover modelling of a mountainous region. We employ the Instructed Glacier Model (IGM) to grow mountain glaciers up to an orogen-scale ice field over several millennia of model years, at different spatial resolutions ranging from 50 to 2000 m. Such computationally expensive experiments would be unfeasible with traditional glacier models, e.g., Elmer Ice (Gagliardini et al., 2013) or the Parallel Ice Sheet Model (PISM; Winkelmann et al., 2011). IGM enables us to overcome this computational bottleneck by using deep learning based on the physics of higher-order 3D ice flow. Although deviations between a full Stokes ice physics implementation and IGM which is based on the Blatter-Pattyn approximation are expected, our focus in this study is on the impact of spatial resolution on bedrock topography and ice model results that ought to exist for any model. In the following, we first describe the glacier model and experimental design. Then, we present the model results, focusing on systematic differences across different spatial resolutions. Our analysis examines ice volume, thickness, velocity, and basal temperature in terms of their spatial and temporal variations. Finally, we discuss the underlying processes driving the spatiotemporal differences in ice cover and dynamics.

2 Methods and Materials

2.1 The Instructed Glacier Model (IGM)

IGM is an open-source Python model that simulates glacier evolution in 3D (Jouvet and Cordonnier, 2023). The ice flow model is based on physics-informed deep learning that achieves high computational efficiency - especially with Graphics Processing Units (GPU). Within run times of 9 days, we were able to apply IGM to our model domain at 50 m resolution with 16,150,000 pixels over a model time of 5000 years. Jouvet and Cordonnier (2023) showed that by directly enforcing physical laws in the learning process, IGM reproduces the solutions of a high-order analytical solver of ice flow with high fidelity. The physics-informed deep learning approach is independent of training data from other glacier models, which allows us to run the same experimental set-up at different spatial resolutions and directly compare the model results. Our setup is based on Leger et al. (2025), where IGM was used to produce a model of the LGM in the Alps that closely matches geological evidence. A direct comparison of a simulation of the European Alps at 2 km resolution using IGM to the respective simulation using the well-tested and widely used Parallel Ice Sheet Model (PISM; Winkelmann et al., 2011) published by Jouvet et al. (2023) showed minor deviations, confirming that the alpine ice field is a suitable application for IGM (Leger et al., 2025). We used the parameterisation from Leger et al. (2025)'s best-scoring simulation (number 37) out of an ensemble of 100 Alps-wide simulations at 300 m resolution. This set-up is therefore well-adopted to the Alps and the formation of an extensive ice field. In the following, we briefly describe the submodules covering essential glacier processes

such as ice flow and surface mass balance as well as avalanching and bed deformation. All model parameters can be found in the supplements (Table S1).

The ice flow module in IGM is designed to efficiently simulate 3D velocities using a physics-informed deep learning approach. Instead of solving costly Stokes equations or approximations thereof, ice velocities are simulated by an inexpensive convolutional neural network (CNN) (for a detailed description see Jouvet and Cordonnier, 2023). The ice velocities are simulated as energy-minimizing solutions of the higher-order Blatter-Pattyn model (Blatter, 1995) which has been shown to reproduce ice velocities that agree well with full Stokes models (Pattyn et al., 2008). The generic emulator is capable of handling a variety of ice flow and temperature regimes which is important for modelling alpine ice fields since mountain glaciers exhibit a range of flow velocities (Millan et al., 2022; Jouvet and Cordonnier, 2023). Ice flow at the ice-bedrock boundary is described by a non-linear Weertman friction condition (e.g., Schoof and Hewitt, 2013). The initial glacial state is based on a pretrained CNN described in Jouvet and Cordonnier (2023) to advance convergence to the Blatter-Patty model in the first time-steps. For this pretraining, the emulator was trained over a diverse catalogue of glaciers and flow regimes at 100 m spatial resolution with 10 vertical layers, fine vertical discretization close to the ice-bedrock interface, 16 CNN-layers, and 32 CNN-output filters (Jouvet and Cordonnier, 2023). For adjustments to new ice field states attained through run time, we retrained the physics-informed neural network multiple times within a single model year (every ~0.18 years). The on-the-run retraining in the highest-resolution simulations at 50 and 100 m was performed more often (every ~0.05 years). The retraining frequencies were found to be high enough to ensure that the emulator's deviation from the analytical solver typically remains below 5 m yr^{-1} in ice velocity (see Figs. 4, 5 in Jouvet and Cordonnier, 2023; Leger et al., 2025). Computations at 50 and 100 m resolutions were executed on a ~7000-core Nvidia A100 GPU, for coarser resolutions we used a Nvidia A40 and A30 GPU.

The enthalpy module follows an energy-conservative formulation by Aschwanden et al. (2012). It distinguishes between cold and temperate ice: For cold ice at temperatures below the pressure-melting point, enthalpy is proportional to pressure-adjusted temperature, while for temperate ice, enthalpy includes an additional component incorporating the creation of water content through energy transfer. The Arrhenius factor in the Blatter-Pattyn model is calculated from pressure-adjusted ice temperature via the Glen-Paterson-Budd-Lliboutry-Duval law (Cuffey and Paterson, 2010). The sliding coefficient follows the Mohr-Coulomb sliding law (Cuffey and Paterson, 2010) and accounts for basalt melt and meltwater production when the pressure melting point is reached. At the ice surface, enthalpy is constrained by surface temperature, which is modified by our temperature forcing (see Sect. 2.2). At the glacier bed, boundary conditions depend on the temperature at the bottom ice layer and bed surface, where we set the geothermal heat flux to 0.065 W m^{-2} across the entire model domain.

The surface mass balance (SMB) computation is based on a temperature-index model (e.g., Hock, 2003) to calculate the SMB from monthly near-surface air temperature and precipitation. Ice surface accumulation is equal to precipitation when air temperatures are below 0 °C and decreases to zero linearly with temperatures between 0 and 2 °C. Ablation is computed with a positive-degree-day model using the integral formulation from Calov and Greve (2005) that accounts for stochastic temperature variations. To prevent ice flow beyond our model domain, we set the SMB to -50 m yr^{-1} at a distance of 5 km from the model domain edges.

Modelling space- and time-dependent bed deflection as a response to ice loading and unloading is realized by coupling IGM with the gFlex model (Wickert, 2015) using the two-dimensional elastic thin-plate equation in Mey et al. (2016). Based on Leger et al. (2025)'s best-scoring ensemble simulation, we assume a lithospheric effective elastic thickness of 45 km and set the frequency of gFlex iterations to 50 years with a spatial resolution of 2 km.

Avalanching impacts ice accumulation, surface elevation, as well as flow velocity and is especially relevant for modelling ice fields at high resolution where slopes are generally steeper (Fig. 1c). The avalanche module in IGM is based on Kessler et al. (2006) and redistributes modelled accumulation downslope until the glacier surface reaches an angle of repose, here set at 45 °. This process is applied at a frequency of five years.

2.2 Experiment design

As we aim to investigate resolution-related ice model differences in mountainous regions, we chose a region with a complex alpine topography featuring high mountain summits as well as deep and narrow valleys. The ice field we modelled is located in the Western Alps, encompassing several mountain massifs with elevations exceeding 4000 m a.s.l. (Fig 1a). This mountainous region provides the glacier bed for a system of small tributary glaciers, which flow over steep terrain with an average slope of 21.5 ° and eventually merge into large and thick valley glaciers (>5 km wide, up to ~100 km long). Our model domain is positioned near the southwestern end of the European Alps, where it is naturally bounded by lowlands to the northwest and southeast. To enhance computational efficiency, we rotated the model domain clockwise by 55° to reduce the number of lowland pixels that do not contribute to the ice cover, constraining the model area to a total of 40,375 km^2 (Fig. 1a). Our modelled ice field on this topography covers a maximum area of ~12,700 km^2, comparable in size to the present-day Southern Patagonian Icefield (~12,200 km^2; Meier et al., 2018). The bedrock topography is taken from the ALOS World 3D 30 m DEM (Tadono et al., 2014), which was resampled to 50 m with present-day glaciers and lakes removed based on Cook et al. (2023). The DEM is resampled to multiples of 100 m resolution between 100 and 1000 m and multiples of 200 m up to 2000 m. For all DEM resampling of input fields, we use cubic convolution due to its higher accuracy in resolving surface elevation and slope angles compared to other resampling methods like bilinear or kriging interpolation (Minh et al., 2024). In all experiments the resolution in the x- and y-directions is equal. Every simulation starts with ice-free conditions.

We used a simplified climate set-up as we aimed to assess the influence of spatial resolution on a growing and melting ice field instead of reconstructing past glaciations. We applied a synthetic temperature forcing that mimics transient cooling and warming within the range of temperature rates that occurred during the last glacial cycle (Jouzel and Masson-Delmotte, 2007), allowing for the build-up of a large ice field like during the LGM. The forcing begins with an initialization phase of 1000 years with no temperature change to ensure that the initial glacial state is in balance with our setup. The initialization phase is followed by linear cooling over 2000 years down to -8 K relative to the starting condition and a warming phase over another 2000 years until the entire cooling is reversed. The cooling and warming rates are -4 and +4 K per 1000 years, respectively, and the total model time is 5000 years. We carried out additional experiments with a slower temperature cooling and warming of -2 and +2 K per 1000 years stretched out over 4000 year-long cooling and warming phases, resulting in a total model time of 9000 years. These simulations were run at 100, 500, and 1000 m spatial resolution. All simulations started with temperature and precipitation conditions similar to the present-day. Monthly temperature and precipitation values are derived from climate data averaged over 1981–2010 from a weather station in Modane, France, located at 1228 m a.s.l. within the model domain (Météo-France, 2022). We used a lapse-rate of 6 °C per 1000 m elevation to project the temperatures across the entire model domain. The resulting mean annual temperature at sea level is ~14.9 °C. With an annual sum of 660 mm, the weather station's precipitation values lie at the lower end of typical values in the European Alps (e.g., Isotta et al., 2014). Therefore, to ensure that the ice field covers the entire mountainous part of the model domain at the time of maximum cooling, we multiplied monthly precipitation values by 1.6, resulting in a more realistic annual precipitation of 1056 mm per year. Those monthly precipitation values were kept constant in space and unchanged throughout the warming and cooling phases.

2.3 Model output analysis

To compare simulations across all resolutions, we resampled all model inputs and outputs to 50 m using nearest-neighbour interpolation to preserve the pixel structure while avoiding artefacts from coarse-resolution resampling. We analysed differences relative to the highest-resolution simulation at 50 m, which serves as our reference. Spatially distributed model results are analyzed within a defined mask that is based on glacial drainage basins located well-inside the model domain at maximum ice coverage of the 50 m simulation. We thus excluded any glacier catchments that lead to ice flow reaching the domain borders to avoid biases in results from our non-mass-conservating domain boundary scheme of ice melt. We used elevation bands of 0–1200, 1200–2400, and >2400 m a.s.l. to distinguish between different altitudes that correspond to deeply incised, gently sloping valleys at low altitudes and steep mountain summits at high altitudes, and a transitional domain, where much of the modelled ice volume is located (Fig. 1c). For a map showing the distribution of the elevation bands across the model domain, we refer to the supplements (Fig. S1). For the purpose of this study, we introduce the notation X_r for any input or output variable X at resolution r (in metres) and denote bedrock elevation with respect to mean sea level.

3 Results

3.1 Topographic variability of resampling effects

The changes in surface elevation due to resampling the 50 m DEM to a coarser resolution are not uniform across the landscapes. Based on the notion that resampling to a coarser resolution affects large and deep valleys less compared to small tributary gorges or ravines, we assessed elevation differences for valleys of distinct Strahler stream order (Strahler, 1957), using a minimum upstream area of 0.5 km^2. The Strahler order defines the stream size based on a hierarchy of tributary streams. Streams of order 1 are the smallest without any tributaries. As the Strahler order increases, the streams and associated valleys have more branches upstream, their upstream area increase and so does the discharge and size of the valley (see Fig. S2). The comparison of variously resampled DEMs to the reference DEM at 50 m resolution shows that elevation differences vary with Strahler order (Fig. 2). The highest discrepancies are at intermediate Strahler orders (3–4), with median difference values ranging from 150 to over 250 m for DEMs resampled to a resolution of 1000 m and coarser compared to the 50 m DEM. In contrast, at very low (1) or high (6–7) Strahler orders, corresponding to small and steep as well as large and gentle valleys, respectively, median difference values are less than 165 m, for any resolution. At streams of low order, bedrock elevation tends to be higher than in the 50 m DEM, though differences extend to more negative values than at any higher stream order. Elevation differences in large valleys of high streams orders (6–7) are small and strictly positive, indicating resampling-induced elevated valley floors. At 300 m resolution and finer, resampling effects are small and median values remain below 50 m, regardless of the stream order. Overall, resampling effects at resolutions of 1000 m and coarser are strong, especially in intermediate valleys, while effects at fine resolutions and in large valleys are minor.

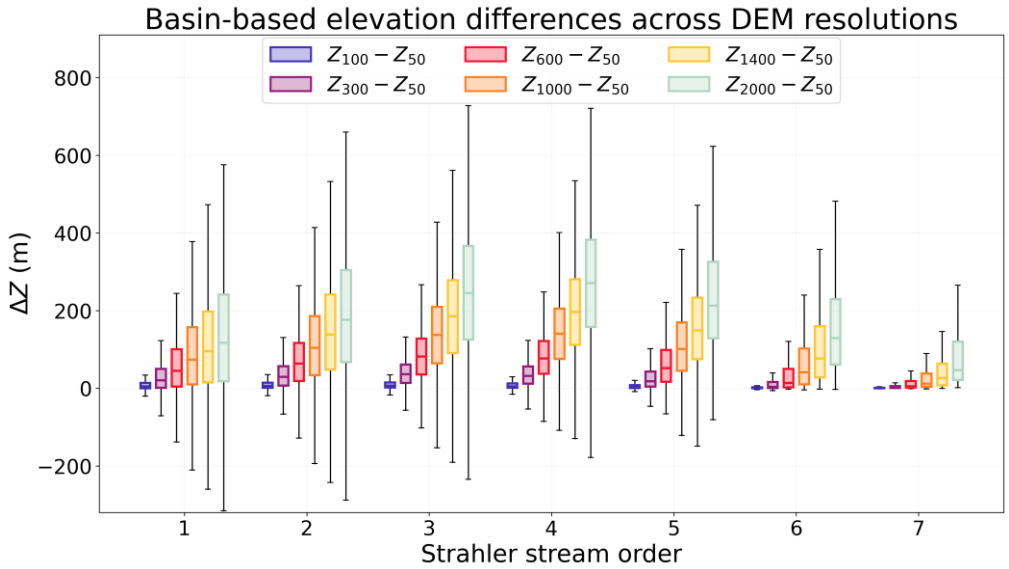

Figure 2 Elevation differences $\Delta Z = Z_r - Z_{50}$ in the Western Alps (see extent in Fig. 1a) between the 50 m DEM and DEMs at resolutions of r = 100 (blue), 300 (purple), 600 (red), 1000 (orange), 1400 (yellow), and 2000 m (grey) by valley type defined by Strahler order (Strahler, 1957). Boxes extend from the first quartile to third quartile with a line at the median. The whiskers extend from the box to the farthest data point lying within 1.5 times the interquartile range from the box.

3.2 Temporal evolution of ice volume and area

Over the entire model duration, a coarser spatial resolution leads to an increase in ice volume, despite similar ice extents (Fig. 3a, b). After the initialization phase (0–1000 years), the 2000 m simulation has ~160 km^2 of ice volume which is more than 10 times that of the 50 m run (~12 km^2). Maximum ice volumes in simulations at 300 m resolution and finer are comparable, and increase steadily at intermediate resolutions (Figs. 3a, S3). At resolutions coarser than 800 m, maximum volumes are consistently high, exceeding 40,000 km^3 and culminating in a factor ~2.5 difference between the 50 and 2000 m simulations. In contrast, maximum ice area values range only slightly between 11,900 to 13,000 km^2.

The modelled ice volumes exhibit pronounced hysteresis effects with respect to the temperature forcing, which are greater at coarser resolution. In all simulations, the timing of maximum ice volume lags behind the strongest cooling of -8 K at 3000 years. However, the delay of peak ice volume is most pronounced at resolutions coarser than 800 m, with a time lag of up to 420 years compared to a delay of less than 200 years at resolutions of 300 m and finer (Figs. 3, S3). We also observe time lags of reaching the maximum ice area, but these are much smaller than for ice volume, yet they still increase with coarser resolution. Larger and persistent volume differences between the warming (3000–5000 years) and cooling phases (1000–3000 years) in the coarse resolution simulations occur for temperature forcings stronger than -3 K and thus during large parts of the model run (~1750–4250 years). At resolutions coarser than 800 m, ice volumes during the warming phase are more than 60 % higher than during the cooling phase under the same temperature forcing relative to the maximum ice volume (Fig. 3c). The shorter delays in reaching the maximum ice volume as well as smaller volume differences between the warming and cooling phases at fine resolutions indicate that fine resolutions capture changes in temperature forcing more accurately.

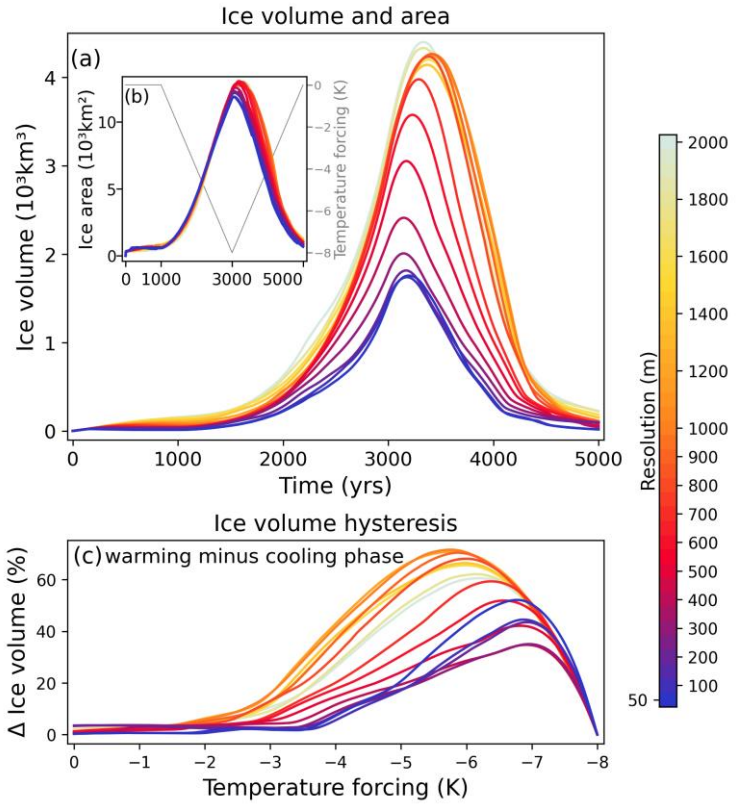

Figure 3 Temporal evolution of (a) ice volume and (b) ice area at resolutions between 50 and 2000 m. The temperature forcing is shown in (b) (grey). (c) Ice volume differences at times with the same temperature forcing value during the warming (3000–5000 years) and cooling phase (1000–3000 years) (warming minus cooling phase) relative to the maximum ice volume in each run. For example, a temperature forcing of -4 K is applied at model year 2000 (cooling phase) and again at year 4000 (warming phase). The relative ice volume difference at -4 K is computed as the difference in ice volume at years 4000 and 2000 relative to the maximum ice volume at each resolution.

The resampling effects on the DEMs that depend on valley sizes (Fig. 2) only partly coincide with changes in ice volume proportions across bedrock altitude (Fig. 4). The distribution of ice volume as well as timing of its maximum is significantly influenced by resolution at mid (1200–2400 m a.s.l.) and low altitudes (0–1200 m a.s.l.). In contrast, at high altitudes (>2400 m a.s.l.) with drainages of generally low Strahler order, resolution-related differences in the topography and ice volume are small (Figs. 2, 4). Around 2000–2500 years, thick glaciers begin to form in large valleys, causing low altitudes to contain more ice volume than high altitudes, although covering less ice area. While resampling effects are minor in large valleys located at low altitudes (Fig. 2), resolution effects on the distribution of ice volume are most pronounced at these altitudes. Ice volume at low altitudes grows relatively slower and contributes less to the total ice volume at coarser resolutions (Fig. 4b). At 1000 m resolution, the maximum share of low-altitude ice volume is about 10 % less than at 50 m resolution. This reduced contribution is compensated for by mid altitudes, which contain relatively more volume in the coarse than in the fine resolution simulation. The time lag between maximum cooling and the onset of ice melt are observed at all altitudes but originates from the low altitudes where the contribution of ice volume and area decreases ~500 years later in the 1000 than in the 50 m simulation. In contrast, for ice area, resolution effects are overall small and rather independent of altitude (Fig. 4a).

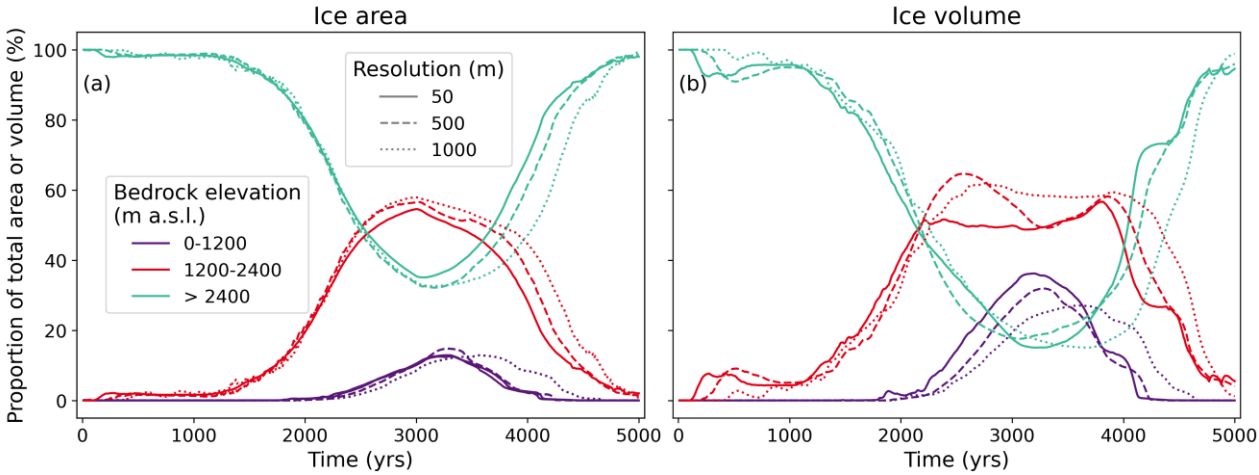

Figure 4 Temporal evolution of the contribution of low (0–1200 m a.s.l., purple), mid (1200–2400 m a.s.l., red), and high (> 2400 m a.s.l., green) bedrock altitudes to (a) total ice-covered area and (b) total ice volume. Results are shown for simulations at 50 (solid lines), 500 (dashed lines), and 1000 m (dotted lines) resolution.

3.3 Ice field conditions at full glaciation

Resolution-related deviations in ice volume that depend on altitude arise from spatially non-uniform ice thickness patterns. At full glaciation, ice thickness maps differences relative to the 50 m reference run reveal distinct spatial patterns between fine and coarse resolutions (Fig. 5; full version in Fig. S4). For comparison, maps of absolute ice thickness are shown in the supplement (Fig. S5). Among resolutions of 300 m and finer, ice thickness is generally comparable, and differences only increase slightly with coarser resolution (Fig. 5a, b). At these resolutions, large valley glaciers are marginally thicker, while small tributary glaciers are slightly thinner than in the 50 m simulation. Differences in ice thickness among the fine resolutions mostly remain below 100 m, except at some glacier termini, where they are related to different extents. For coarser resolutions, ice thickness differences increase significantly and are generally positive (Fig. 5c–f). Although the main valleys are less affected by resampling (Fig. 2), the glaciers filling these valleys are most affected by coarser resolution, with thickness differences reaching a few hundreds of meters. Negative differences are exceptions and restricted to glacier termini. At the coarsest resolutions, the spatial pattern of high thickness differences in major valleys is less pronounced and negative differences appear more often (Fig. 5f). This indicates that ice thickness differences do not increase monotonically with coarser resolution at every pixel.

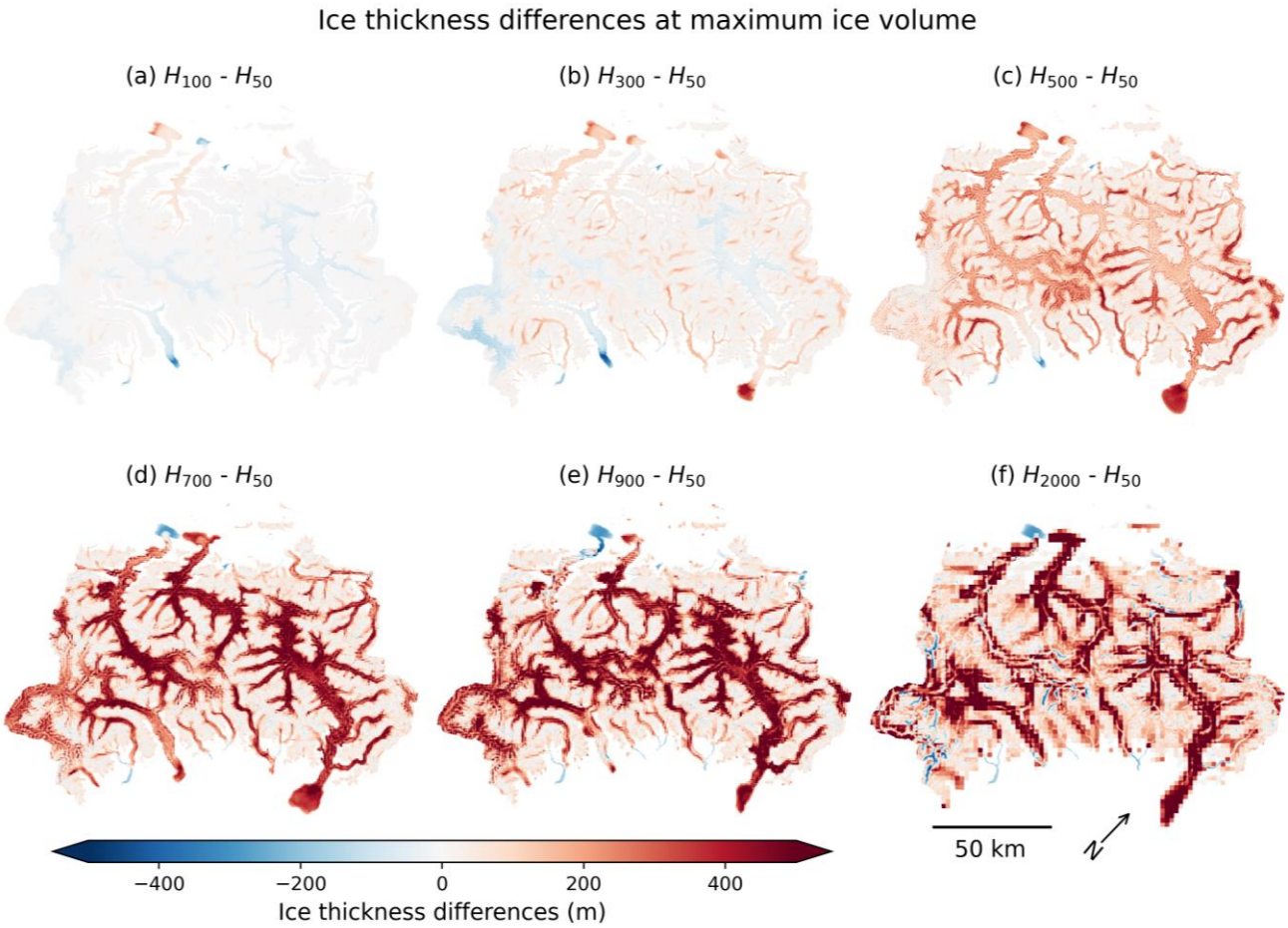

Figure 5 Ice thickness differences ($\Delta H = H_r - H_{50}$) between simulations at resolution r = 100, 300, 500, 700, 900, 2000 m and the 50 m reference run, each at the time step of maximum ice volume. Blue colours indicate thicker ice in the 50 m run; red colours indicate thicker ice at the coarser resolution r.

A visualization of ice thickness with underlying bedrock along a transect reveals resolution-related differences in smaller-scale features of ice surface elevation (Fig. 6). At fine resolution, thick glaciers show smooth surfaces, even though the underlying bed is rough (Fig. 6a). However, at coarser resolutions, the ice surface is rugged with larger variations in ice thickness, despite overall thicker ice. This unrealistic imprint of bedrock topography in the ice surface increases with coarser resolution. The highest mountains are covered by relatively thin ice in all simulations. However, while ice thickness on nunataks (exposed summits surrounded by ice) is typically ~5 m in the 50 m run, it increases to more than 100 m in the simulation at 1000 m resolution (Fig. 6). Large valleys such as the Aosta Valley are filled with thicker ice at coarser resolutions, allowing the ice to reach higher elevations. As a result, the Aosta Valley glacier in the transect is connected to tributary glaciers from the valley sides at 1000 m resolution that are absent in the 50 m run (Fig. 6).

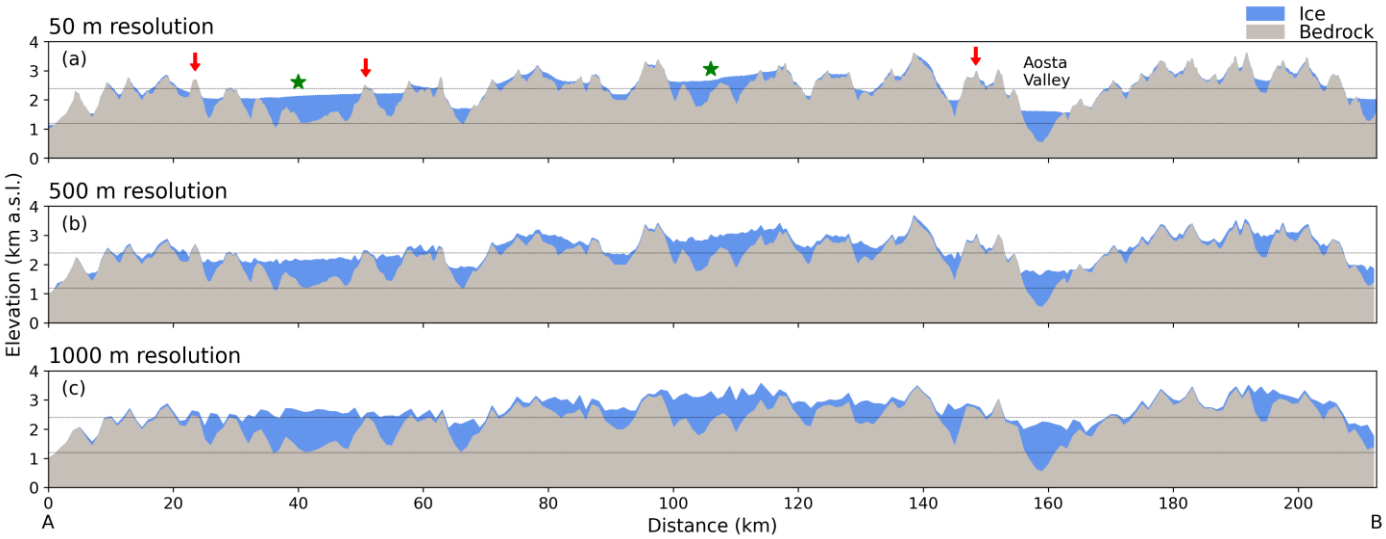

Figure 6 Bedrock (grey) and ice thickness (blue) at the time of maximum ice volume across the transect between points A and B shown in Fig. 1a at (a) 50, (b) 500, and (c) 1000 m resolution. Red arrows mark exemplary nunataks with thin ice in the 50 m resolution run and high ice thickness at coarser resolution. Glaciers marked with green stars are smooth in the 50 m run but rugged at coarser resolution. Vertical lines at 1200 and 2400 m a.s.l. mark our defined thresholds for low (0–1200 m a.s.l.), mid (1200–2400 m a.s.l.), and high altitudes (<2400 m a.s.l.) in Figs. 4, 8, and 9.

A closer look at the distribution of ice across bedrock elevations shows how thickness and area influence ice volume at different spatial resolutions (Fig. 7). Most of the ice field's area is located at ~2200 m a.s.l. irrespective of resolution, dropping off quickly with lower elevation (Fig. 7a). However, because the mean ice thickness simultaneously increases with lower elevations in all simulations, the ice volume attains maximum values at mid altitudes. The elevation range for high ice volume spans ~500–2200 m a.s.l. at fine resolutions, but it is more focused in the range ~1300–2200 m a.s.l. at resolutions coarser than 800 m (Fig. 7b). This shift is largely due to the general thicknening of the ice in coarser resolution models. Whereas resolutions of ~300 m and finer produce mean thickness of similar magnitude and distributions across bedrock altitudes, resolutions coarser than ~800 m show much higher thickness that are comparable among these coarse resolutions, with large changes at intermediate resolutions. (Fig. 7c). At ~1500 m a.s.l., thicker glacier combined with an additional increase in ice area to produce over 160 % more ice volume at resolutions coarser than 800 m compared to the 50 m run. The strong increase in ice volume at mid altitudes is unmatched at other elevations and reflects the relative redistribution from low to mid altitudes at coarse resolutions, already indicated in Fig. 4. At low elevations of ~500 m a.s.l., the mean thickness of large valley glaciers increases significantly with coarser resolutions. However, these differences play a minor role in the total ice volume changes due to the limited number of large valley glaciers.

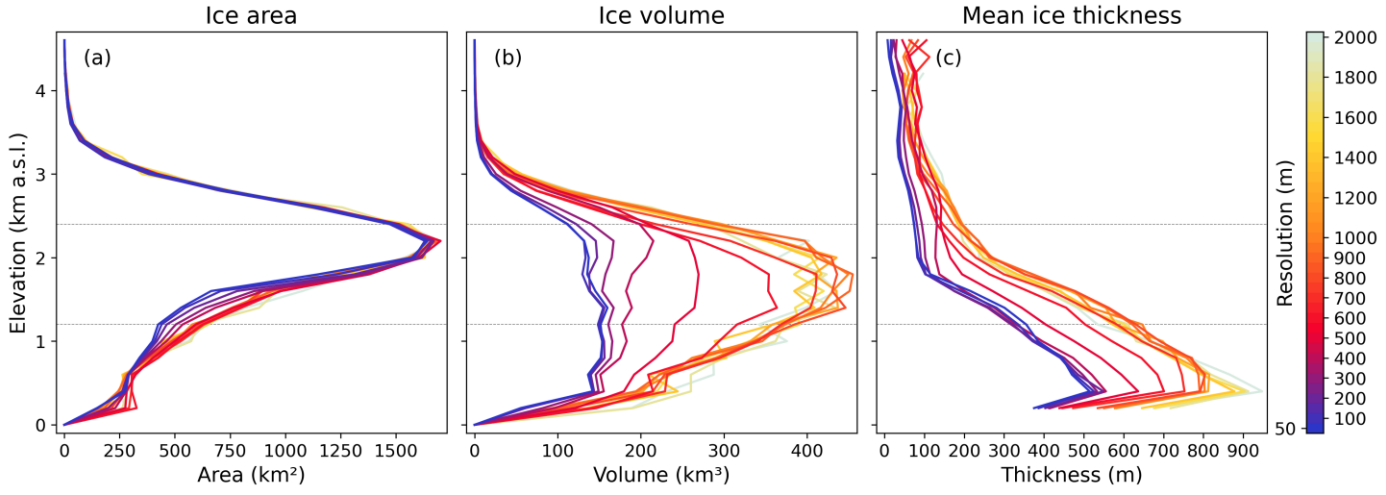

Figure 7 (a) Ice area, (b) ice volume, and (c) mean ice thickness across bedrock elevation for simulations at resolution *r*. All values are calculated at the time of maximum ice volume for each run, and with respect to 200 m elevation bins of the corresponding DEMs at resolution *r*. Dashed

horizontal lines in grey at 1200 and 2400 m a.s.l. mark our defined thresholds for low (0–1200 m a.s.l.), mid (1200–2400 m a.s.l.), and high altitudes (<2400 m a.s.l.) in Figs. 4, 8, and 9.

Non-linear resolution effects are observed for various variables that describe the mean state and dynamics of the ice field (Fig. 8). The magnitude of these changes varies with bedrock altitude, as already seen for ice thickness and volume (Figs. 5, 7). Despite non-linear changes in model outputs, differences in input DEM elevation and slope compared to the 50 m reference run vary monotonically with resolution and are negligible for fine resolutions up to 300 m (Fig. 8a, b). Modelled ice volume and mean thickness at maximum glaciation are comparable at fine resolutions but increase strongly at intermediate resolutions before levelling off at coarse resolutions. This pattern is most distinct at mid and low altitudes (Fig. 8c, d). Specifically, ice thickness differences between the 50 and 300 m runs are only a few percent and become much higher between the 300 and 800 m simulations, with differences of ~65 % at low and ~175 % at mid altitudes. The largest absolute differences in mean ice thickness of over 300 m (74 %) between the coarsest and finest simulations are observed at low altitudes, while relative differences are highest at high elevations and reach ~150 % (absolute differences of 100 m). The particularly strong increase in ice volume at mid altitudes originates from large differences in mean ice thickness that integrate over a large glacial area, as shown in Fig. 7.

Apart from geometrical differences, we also observe non-linear resolution-related changes in the ice field's dynamics, with generally slower flow velocities at coarser resolution (Fig. 8e). Average velocity differences at low and mid altitudes are small at the finest resolutions and most pronounced at resolutions between 400 and 800 m, with substantial reduction in ice velocities. For instance, at low altitudes, where glaciers flow fastest, mean velocity values drop from over 200 m yr^{-1} at 500 m resolution to less than 150 m yr^{-1} at resolution coarser than 800 m. At these altitudes, average values increase slightly among resolutions of 300 m and finer, which is noteworthy because an increase in average velocities with coarser resolution is only observed at these altitudes.

Finally, resolution-related changes in the thermal regimes are most pronounced at high altitudes (Fig. 8f). Average ice temperatures at the glacier base transition from cold-based (with a mean basal ice temperature of -4.8 °C at 50 and 100 m resolution) to temperate conditions at resolutions coarser than 1000 m. Similarly, at mid altitudes, basal ice is colder at fine resolutions, with mean temperatures shifting from ~-0.8 °C to 0 °C by 800 m resolution, while basal ice generally remains temperate at low altitudes across all resolutions. Overall, ice field characteristics during full glaciation shift from relatively thin and fast-flowing glaciers at fine resolutions (~50–300 m) to thick, slow flowing and generally temperate ice at coarse resolution (~800–2000 m).

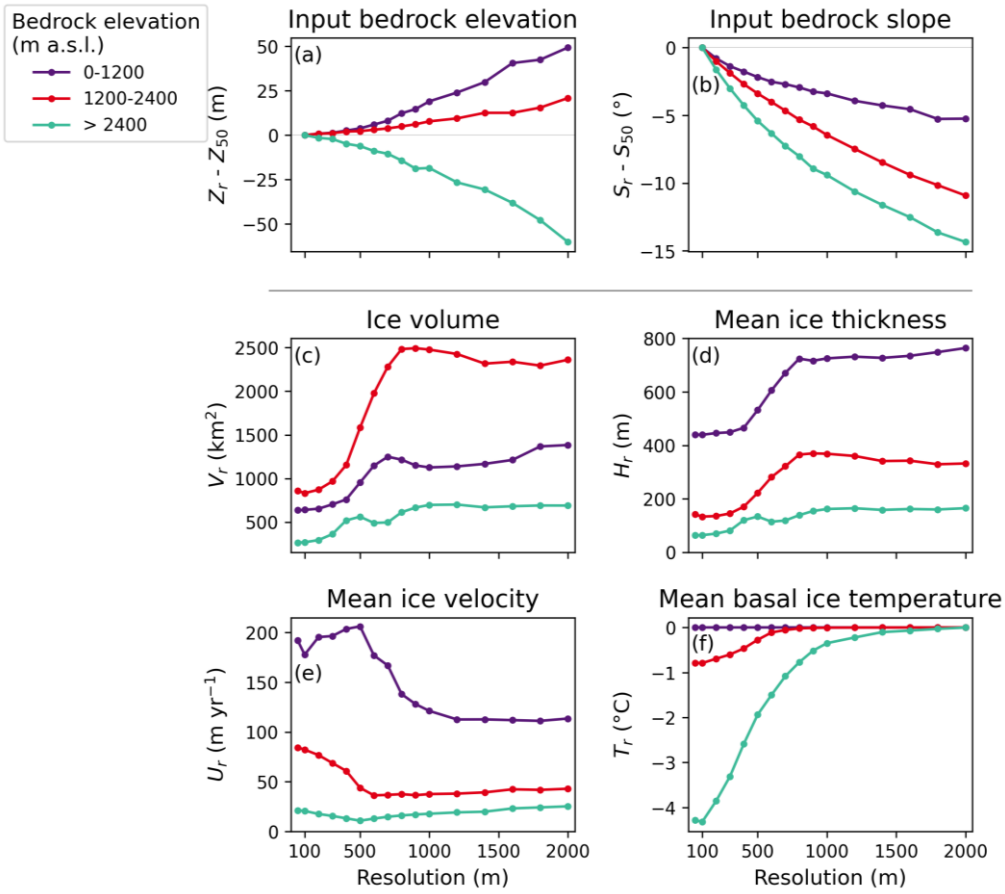

Figure 8 Comparison of model inputs and outputs at low, (0–1200 m a.s.l., purple), mid, (1200–2400 m a.s.l., red), and high altitudes (> 2400 m a.s.l., green). Mean differences of (a) bedrock elevation ($\Delta Z = Z_r - Z_{50}$) and (b) bedrock slope ($\Delta S = S_r - S_{50}$) of the input DEMs at resolution *r* compared to the 50 m DEM. All means in (a) and (b) are taken over the glaciated area at 50 m and resolution *r*, and bedrock altitudes are defined with respect to the 50 m DEM. Model output variables are shown in (c)–(f) below the vertical line and refer to the time of maximum ice volume in each simulation at resolution *r*: (c) ice volume (V_r), (d) mean ice thickness (H_r), (e) mean depth-averaged ice velocity (U_r), (f) mean pressure-adjusted basal ice temperature (T_r). All means in (c)–(f) are taken over the glaciated area at resolution *r* and bedrock altitudes are defined with respect to the DEM at resolution *r*.

3.4 Impact of temperature forcing rate

A comparison of modelled ice volume under fast (± 4 K/kyrs) and slow (± 2 K/kyrs) temperature forcing shows that coarser resolution results depend more on the rate of cooling, while results at fine resolutions are rather comparable, despite different speed of temperature forcing (Fig. 9). The maximum ice volume increases with the slow compared to the fast temperature forcing for all resolutions. This increase is most pronounced at coarse resolutions, with ~25 % more ice volume using the slow cooling rate in the 1000 m resolution run, whereas the increase is only 12 % at 100 m resolution. Most of the added ice volume originates from low altitudes (Fig. 9c). However, ice volume differences that are related to spatial resolution are more pronounced than those caused by the change in temperature forcing rate. In particular, the peak ice volume more than doubles between the 50 and 2000 m simulations, with 138 % more volume under fast and 162 % under slow forcing.

Despite these differences, the distribution of ice volume across altitude bands remains largely unchanged and most of the ice volume is contained at mid altitudes in all simulations (Fig. 9b). The shift of ice volume distribution from low to mid altitudes with coarser resolutions at full glaciation (Fig. 4) is persistent under slower temperature forcing but reduced from 10 % to ~5 % under fast temperature forcing. Under both temperature forcings, ice volume at high altitudes changes more gradually, while low-altitude regions respond with abrupt and strong increases and decreases. The delay in reaching the maximum ice volume with respect to temperature forcing is significantly reduced with the slower temperature change. In the 1000 m runs, the lag drops from 420 to

250 years, driven by continued ice growth at low altitudes, while glaciers at mid and high altitudes are more sensitive to temperature change and start to retreat earlier. In comparison, the maximum ice volume in the 100 m run is reached only ~200 years after the peak cooling under both forcings. Note, however, that the x-axis of Fig. 9 contains twice as much absolute time for the slower compared to the faster temperature forcing, partly masking that resolution-related time lags remain. Reduced hysteresis effects are also apparent in lower volume differences between the warming and cooling phases using the slower forcing, especially at coarse resolutions (Fig. S7).

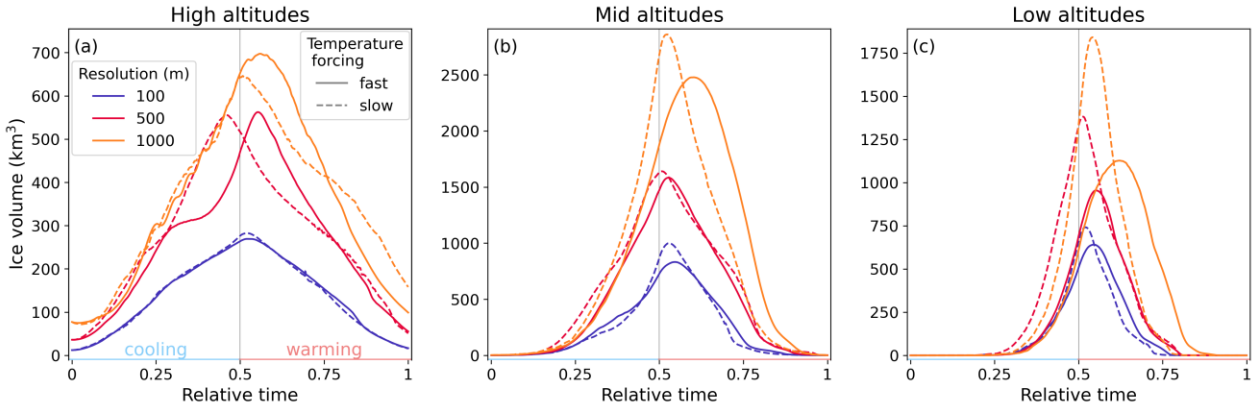

Figure 9 Ice volume under fast (±4 K/kyrs, solid line) and slow (±2 K/kyrs, dashed line) temperature forcing at 100 (blue), 500 (red), and 1000 m (orange) resolution at (a) low (0–1200 m a.s.l.), (b), mid (1200–2400 m a.s.l.), and (c) high bedrock altitudes (>2400 m a.s.l.). The x-axes show relative time, from 0 (start of cooling phase with a temperature forcing of 0 K) to 1 (end of cooling phase with a temperature forcing of 0 K). At 0.5, half of the simulation is reached, where temperature forcing is strongest at -8 K and the warming phase begins. In model years, the cooling and warming phases span 2000 years each under fast and 4000 years each under slow temperature forcing.

4 Discussion

4.1 Resolution-related differences across bedrock altitude

Our results show that ice is generally thinner and faster-flowing at resolutions of 300 m and finer, in contrast to rather thick glaciers at resolutions coarser than 800 m, with strong changes at intermediate resolutions. We relate these differences between fine and coarse resolution simulations to a combination of resampling effects in the input DEMs, glacier dynamics and feedback mechanisms. Generally, ice growth is supported by the coarse-resolution topography with flattened mountain peaks and gentle slopes, while fine resolutions accurately resolve topographic details which promotes ice flow speed-up and thinning in steeper and narrower valleys.

At high altitudes, glaciers are generally thin and less extensive, leading to small absolute differences in thickness and velocity which are nonetheless significant in relative terms. Although the coarse-resolution topography has less area at the highest elevations (Fig. 1), which generally restricts ice accumulation, ice is thicker at coarser resolutions (Figs. 5, 7, 8). This ice build-up is likely caused by gentle slopes in the coarse resolution DEMs which contribute to preventing glaciers from directly flowing into the ablation area. The shift from generally frozen bed conditions at fine resolution simulations to temperate basal ice at coarser resolutions is possibly a consequence of two mechanisms: colder climatic conditions in the fine resolution DEMs due to higher surface elevations, and increased thickness at coarser resolutions resulting in a higher likelihood for basal melting due to increased basal pressure and thus a lower pressure melting point.

In the valleys, ice flow at fine resolutions likely undergoes strong lateral confinement by steeper and narrower valley walls that forces the ice into a more constricted flow path. To satisfy mass conservation for ice as an incompressible fluid, this leads to accelerating ice flow and thus glacier thinning (Leger et al., 2025; Cuzzone et al., 2019). In contrast, at coarse resolutions, thicker ice flows more slowly over smoother topography with gentler slopes (Fig. 7, 8). Among the finest resolutions, the reduction in ice

velocity (Fig. 8) might result from increased lateral shear stress from very steep and narrow valley walls that impose resistance. Within valleys, the surface mass balance-elevation feedback plays an important role: When ice thickness increases, the ice surface reaches higher elevations with lower temperatures, which promotes further ice growth (Levermann and Winkelmann, 2016). This feedback is most likely strongest in valleys with steep and narrow sidewalls at fine resolution and partly offsets ice thinning due to acceleration from channelized flow, indicated by consistently thicker ice at low altitudes than at high and mid altitudes - across all resolutions (Figs. 7, 8). At coarser resolutions, valley floors are elevated due to DEM resampling (Figs. 1, 2, 8), thereby expanding the accumulation zone and further enhancing ice build-up.

4.2 Hysteresis effects

Our simulations show that the glaciers' response to changes in temperature are more accurately captured in the fine resolution simulations, where glaciers react more rapidly to transitions from cooling to warming periods (Figs. 3c, 9). Conversely, the delay in reaching maximum ice volume seems augmented in coarser simulations and results are more dependent on temperature forcing rates. These hysteresis effects originate primarily from low-altitude regions (Fig. 4) and highlight the influence of the surface mass balance-elevation feedback, which allows valley glaciers to continue thickening despite rising temperatures. The thicker glaciers with underlying gentler slopes in the DEM at coarse resolution (Figs. 1, 8) result in generally shallower surface gradients (Fig. S6), thereby increasing the glacial response time compared to simulations at fine resolution (e.g., Cuffey and Paterson, 2010). For investigating more rapid climate change events in the geologic past or anthropogenic future with temperature variations of several degrees over centennial to millennial time scales, such as the Bølling-Allerød warming or the Younger Dryas cooling period (Rasmussen et al., 2006; Golledge et al., 2008; Norris et al., 2024; Patton et al., 2017), our results suggest that fine-resolution modelling is crucial to accurately capture the timing of glacial retreat and advances, while avoiding overestimated hysteresis effects.

4.3 Topographic control on resolution-related differences in glacial modelling

Our results demonstrate that the accuracy of numerical models does not increase monotonically with spatial resolution. Similar to Williams et al. (2025) and Rückamp et al. (2020), we identify a spatial resolution that is sufficiently fine to produce results much closer to a fine-resolution reference run than those obtained at coarser resolution. However, instead of a km-scale resolution adequate for Greenland and Antarctica (Williams et al., 2025; Rückamp et al., 2020), we find that modelling the exemplary ice field in the Western Alps requires a resolution of 300 m or finer. At such fine resolutions, the characteristic alpine topography is preserved with high accuracy (Figs. 1, 2, 8). The minor differences in elevation and slope effectively result in similar modelling results (Leger et al., 2025; Williams et al., 2025; Rückamp et al., 2020). However, the non-linear variations in model outputs at coarser resolutions cannot be explained exclusively by gradual changes in DEMs with resolution (Fig. 8 a, b). We argue that the interplay of topographic representation and ice dynamics causes these variations. For example, the ice build-up caused by raised valley floors at coarse resolutions is amplified by the surface mass balance-elevation feedback. We hypothesize that at ~800 m resolution, the topographic constraints become sufficiently weakened so that further coarsening has a minor additional effect. At these resolutions, glacier geometry is increasingly controlled by surface elevation in terms of ice thickness rather than bedrock relief, which is enhanced by the surface mass balance-elevation feedback. At intermediate resolutions of 400–800 m, continuous and large changes with resolution mark the transition between the topographically- and thickness-controlled ice dynamics.

Additional experiments with smoothed topographies that are on average 10 ° less steep than the present-day Alps and mean slopes similar to mountain ranges like, e.g., the Scottish Highlands (e.g., Whitbread et al., 2015) show that spatial resolution has a similar influence on ice dynamics which is again dependent on bedrock altitudes (Figs. S8, S9). In these experiments, we observe strong variations between ~500–700 m resolution (Fig. S9) and comparable results at resolutions of 400 m and finer, which are only slightly

coarser compared to simulations using the original DEM. This emphasizes the importance of running simulations at resolutions at least finer than km- and ideally 400-m-scale, even in relatively smooth mountainous terrain. We expect similar resolution-dependent patterns at high, mid and low altitudes in other mountainous regions, where specific altitude bands may shift depending on regional topographic features.

To overcome resolution-dependent errors in ice modelling, it is necessary to identify a sufficiently fine resolution to model a topographically controlled rather than a too smooth and thick ice field. However, even seemingly stable results at coarse resolutions (900–2000 m) do not indicate that the chosen resolution is sufficient, because model outputs show large variations at intermediate resolutions (400–800 m). A series of tests and considerations of spatial difference patterns might help to detect a sufficiently fine resolution and ensure that an even finer resolution does not substantially influence the ice dynamics. Specifically, checking if surfaces of glacier flowing over mountain summits are realistically represented might be an initial indicator, as models at coarse resolutions might show imprints of bedrock topography onto the ice surface (Fig. 6). Similar features can be observed in other numerical models of glaciations in the European Alps at 1–2 km resolution (Fig. 5 in Leger et al., 2025; supplementary data in Jouvet et al., 2023 and Seguinot et al., 2018). Such tests can be performed on small subsets and therefore require limited computational resources. Without thorough consideration of resolution, however, the model parameters may be tuned to produce seemly accurate glacier geometries that, in fact, compensate for unrealistic terrain representations in too coarse DEMs.

4.4 Limitations of the employed modelling

At fine resolutions that are required to accurately model ice field dynamics, the Blatter-Pattyn approximation implemented in IGM may deviate from the full Stokes solution and exhibit mechanical inaccuracies, particularly in steep terrain (Rückamp et al., 2022; Yan et al., 2023; Hindmarsh, 2004). The presented study deliberately focuses on numerical rather than mechanical errors and demonstrated that substantial numerical errors already occur at spatial resolutions commonly used in large-scale mountain ice-cover simulations (Mey et al., 2016; Seguinot et al., 2018; Jouvet et al., 2023; Golledge et al., 2012; Zhang et al., 2022). For a Greenland ice stream region modelled by Rückamp et al. (2022), velocity deviations between the Blatter-Pattyn and full Stokes model of less than ~10 m yr^{-1} appear smaller than the resolution-induced differences of up to several tens of meters per year in our analysis. Therefore, adopting a full Stokes formulation would substantially increase computational costs without addressing the main source of error. Future studies are needed to systematically assess the benefits of full Stokes models at fine resolutions in alpine regions.

For practical considerations, we argue that improving numerical accuracy through finer spatial resolution is a necessary prerequisite before resorting to mechanically more sophisticated ice-flow models. Additional model components such as incorporating erosion processes, potentially enhance resolution-related effects by altering valley shapes (Liebl et al., 2021; Valla et al., 2011). The accelerated ice flow in fine-resolution models is expected to enhance the carving of larger trunk valleys, whereas thin and bed-frozen ice-covers shield high altitude plateaus from erosion processes, and ice-free parts are exposed to non-glacial erosion (Bernard et al., 2025; Egholm et al., 2017). Continued model development is essential to allow for higher-resolution modelling over large time and spatial scales at reasonable computational costs, for example through GPU-based approaches.

5 Conclusions

To assess the impact of spatial resolution on model outputs, we simulated the hypothetical growth and decline of a large mountainous ice field in parts of the European Alps over multi-millennial time scales at different resolutions ranging from 50 to 2000 m. The simulations over both, large spatial scale and several millennia were made possible by the GPU-based architecture of the Instructed

Glacier Model (IGM). Although total glaciated areas are similar across all resolutions, differences in ice thickness and thus volume are substantial, with high variations between resolutions of 300 m and 800 m. These differences are unequally distributed across the terrain. At high altitudes, coarse resolutions result in flatter mountain tops and shallower slopes that provide a larger accumulation area and thus thicker and slower flowing ice. At maximum glaciation, the ice is typically warm-based at coarse resolutions, while the thinner glaciers on steeper and higher mountains in fine-resolution runs remain cold-based. Elevated valley floors in the coarse-resolution runs enhance ice thickness increase via the surface mass balance-elevation feedback. Large and deeply incised valleys at low altitudes are less affected by resampling to a coarser resolution but their glaciers thicken substantially, while ice flow at fine resolutions is accelerated, resulting in generally thinner valley glaciers. Glacial response time is also affected by spatial resolution, with thicker glaciers at coarse resolutions responding more slowly to temperature changes and exhibiting stronger hysteresis effects. This behaviour depends on the rate of temperature change but persists for the tested cooling and warming rates of 2 and 4 K/kyr.

We conclude that for a mountain range like the European Alps, a resolution of 300 m or finer is sufficient to resolve bedrock slopes, resulting in a more topographically constrained ice field. Seemingly stable model outputs at coarse resolution may be misleading and arise from ice dynamics driven by inaccurately resolved topography. Experiments using a smoothed DEM suggest that the non-linear, altitudinal-dependent influence of spatial resolution are also expected across other mountain regions that are less steep than the European Alps.

6 Code and data availability

The Instructed Glacier Model (IGM) source code (Python programming language) and documentation are available from Guillaume Jouvet's GitHub repository at https://github.com/jouvetg/igm. We used IGM version 2.2.1 and commit 19bf4151d77f97841aacd8d0b743096e48863970. The IGM model set-up from Leger et al. (2025) used in this study is accessible via https://zenodo.org/records/14275231.

7 Author contributions

Conceptualization: HW, DS, support from TPML, GJ. Methodology: HW, DS, TPML, GJ. Investigation: HW, support from DS. Visualization: HW, support from DS and TPML. Supervision: DS, support from RW. Writing (original draft): HW, support from DS. Writing (review and editing): HW, DS, TPML, GJ, RW.

8 Competing interests

The authors declare that they have no conflict of interest.

9 Acknowledgements

This study was supported by the German Research Foundation (DFG) grant to Dirk Scherler (SCHE 1676/6-1) and Ricarda Winkelmann under the priority program "Mountain Building Processes in Four Dimensions (MB-4D)" and by the European Research Council under the European Union's Horizon 2020 research and innovation programme under grant agreement 759639. This work utilized high-performance computing resources made possible by funding from the Ministry of Science, Research and Culture of the State of Brandenburg (MWFK) and are operated by the IT Services and Operations unit of the Helmholtz Centre Potsdam.

10 References

Aschwanden, A., Bueler, E., Khroulev, C., and Blatter, H.: An enthalpy formulation for glaciers and ice sheets, J. Glaciol., 58, 441–457, https://doi.org/10.3189/2012JoG11J088, 2012.

Aschwanden, A., Fahnestock, M. A., and Truffer, M.: Complex Greenland outlet glacier flow captured, Nat Commun, 7, 10524, https://doi.org/10.1038/ncomms10524, 2016.

Bernard, M., Van Der Beek, P. A., Pedersen, V. K., and Colleps, C.: Production and Preservation of Elevated Low-Relief Surfaces in Mountainous Landscapes by Pliocene-Quaternary Glaciations, AGU Advances, 6, e2024AV001610, https://doi.org/10.1029/2024AV001610, 2025.

Blatter, H.: Velocity and stress fields in grounded glaciers: a simple algorithm for including deviatoric stress gradients, J. Glaciol., 41, 333–344, https://doi.org/10.3189/S002214300001621X, 1995.

Calov, R. and Greve, R.: A semi-analytical solution for the positive degree-day model with stochastic temperature variations, J. Glaciol., 51, 173–175, https://doi.org/10.3189/172756505781829601, 2005.

Cook, S. J., Jouvet, G., Millan, R., Rabatel, A., Zekollari, H., and Dussaillant, I.: Committed Ice Loss in the European Alps Until 2050 Using a Deep-Learning-Aided 3D Ice-Flow Model With Data Assimilation, Geophysical Research Letters, 50, e2023GL105029, https://doi.org/10.1029/2023GL105029, 2023.

Cuffey, K. and Paterson, W. S. B.: The physics of glaciers, 4th ed., Butterworth-Heinemann/Elsevier, Burlington, MA, 693 pp., 2010.

Cuzzone, J. K., Schlegel, N.-J., Morlighem, M., Larour, E., Briner, J. P., Seroussi, H., and Caron, L.: The impact of model resolution on the simulated Holocene retreat of the southwestern Greenland ice sheet using the Ice Sheet System Model (ISSM), The Cryosphere, 13, 879–893, https://doi.org/10.5194/tc-13-879-2019, 2019.

Duncan, C., Masek, J., and Fielding, E.: How steep are the Himalaya? Characteristics and implications of along-strike topographic variations, Geol, 31, 75, https://doi.org/10.1130/0091-7613(2003)031%253C0075:HSATHC%253E2.0.CO;2, 2003.

Egholm, D. L., Jansen, J. D., Brædstrup, C. F., Pedersen, V. K., Andersen, J. L., Ugelvig, S. V., Larsen, N. K., and Knudsen, M. F.: Formation of plateau landscapes on glaciated continental margins, Nature Geosci, 10, 592–597, https://doi.org/10.1038/ngeo2980, 2017.

Gagliardini, O., Zwinger, T., Gillet-Chaulet, F., Durand, G., Favier, L., De Fleurian, B., Greve, R., Malinen, M., Martín, C., Råback, P., Ruokolainen, J., Sacchettini, M., Schäfer, M., Seddik, H., and Thies, J.: Capabilities and performance of Elmer/Ice, a new-generation ice sheet model, Geosci. Model Dev., 6, 1299–1318, https://doi.org/10.5194/gmd-6-1299-2013, 2013.

Golledge, N. R., Hubbard, A., and Sugden, D. E.: High-resolution numerical simulation of Younger Dryas glaciation in Scotland, Quaternary Science Reviews, 27, 888–904, https://doi.org/10.1016/j.quascirev.2008.01.019, 2008.

Golledge, N. R., Mackintosh, A. N., Anderson, B. M., Buckley, K. M., Doughty, A. M., Barrell, D. J. A., Denton, G. H., Vandergoes, M. J., Andersen, B. G., and Schaefer, J. M.: Last Glacial Maximum climate in New Zealand inferred from a modelled Southern Alps icefield, Quaternary Science Reviews, 46, 30–45, https://doi.org/10.1016/j.quascirev.2012.05.004, 2012.

Hartmeyer, I., Delleske, R., Keuschnig, M., Krautblatter, M., Lang, A., Schrott, L., and Otto, J.-C.: Current glacier recession causes significant rockfall increase: the immediate paraglacial response of deglaciating cirque walls, Earth Surf. Dynam., 8, 729–751, https://doi.org/10.5194/esurf-8-729-2020, 2020.

Hindmarsh, R. C. A.: A numerical comparison of approximations to the Stokes equations used in ice sheet and glacier modeling, Journal of Geophysical Research: Earth Surface, 109, https://doi.org/10.1029/2003JF000065, 2004.

Hock, R.: Temperature index melt modelling in mountain areas, Journal of Hydrology, 282, 104–115, https://doi.org/10.1016/S0022-1694(03)00257-9, 2003.

Huggel, C., Muccione, V., Carey, M., James, R., Jurt, C., and Mechler, R.: Loss and Damage in the mountain cryosphere, Reg Environ Change, 19, 1387–1399, https://doi.org/10.1007/s10113-018-1385-8, 2019.

Hugonnet, R., McNabb, R., Berthier, E., Menounos, B., Nuth, C., Girod, L., Farinotti, D., Huss, M., Dussaillant, I., Brun, F., and Kääb, A.: Accelerated global glacier mass loss in the early twenty-first century, Nature, 592, 726–731, https://doi.org/10.1038/s41586-021-03436-z, 2021.

Immerzeel, W. W., Lutz, A. F., Andrade, M., Bahl, A., Biemans, H., Bolch, T., Hyde, S., Brumby, S., Davies, B. J., Elmore, A. C., Emmer, A., Feng, M., Fernández, A., Haritashya, U., Kargel, J. S., Koppes, M., Kraaijenbrink, P. D. A., Kulkarni, A. V., Mayewski, P. A., Nepal, S., Pacheco, P., Painter, T. H., Pellicciotti, F., Rajaram, H., Rupper, S., Sinisalo, A., Shrestha, A. B., Viviroli, D., Wada, Y., Xiao, C., Yao, T., and Baillie, J. E. M.: Importance and vulnerability of the world's water towers, Nature, 577, 364–369, https://doi.org/10.1038/s41586-019-1822-y, 2020.

Isotta, F. A., Frei, C., Weilguni, V., Perčec Tadić, M., Lassègues, P., Rudolf, B., Pavan, V., Cacciamani, C., Antolini, G., Ratto, S. M., Munari, M., Micheletti, S., Bonati, V., Lussana, C., Ronchi, C., Panettieri, E., Marigo, G., and Vertačnik, G.: The climate of daily precipitation in the Alps: development and analysis of a high-resolution grid dataset from pan-Alpine rain-gauge data, International Journal of Climatology, 34, 1657–1675, https://doi.org/10.1002/joc.3794, 2014.

Ivy-Ochs, S.: Glacier variations in the European Alps at the end of the last glaciation, CIG, 41, 295–315, https://doi.org/10.18172/cig.2750, 2015.

Jouvet, G. and Cordonnier, G.: Ice-flow model emulator based on physics-informed deep learning, J. Glaciol., 69, 1941–1955, https://doi.org/10.1017/jog.2023.73, 2023.

Jouvet, G., Cohen, D., Russo, E., Buzan, J., Raible, C. C., Haeberli, W., Kamleitner, S., Ivy-Ochs, S., Imhof, M. A., Becker, J. K., Landgraf, A., and Fischer, U. H.: Coupled climate-glacier modelling of the last glaciation in the Alps, J. Glaciol., 69, 1956–1970, https://doi.org/10.1017/jog.2023.74, 2023.

Jouzel, J. and Masson-Delmotte, V.: EPICA Dome C Ice Core 800KYr deuterium data and temperature estimates, https://doi.org/10.1594/PANGAEA.683655, 2007.

Kamleitner, S., Ivy-Ochs, S., Monegato, G., Gianotti, F., Akçar, N., Vockenhuber, C., Christl, M., and Synal, H.-A.: The Ticino-Toce glacier system (Swiss-Italian Alps) in the framework of the Alpine Last Glacial Maximum, Quaternary Science Reviews, 279, 107400, https://doi.org/10.1016/j.quascirev.2022.107400, 2022.

Kessler, M. A., Anderson, R. S., and Stock, G. M.: Modeling topographic and climatic control of east-west asymmetry in Sierra Nevada glacier length during the Last Glacial Maximum, J. Geophys. Res., 111, 2005JF000365, https://doi.org/10.1029/2005JF000365, 2006.

Korup, O., Schmidt, J., and McSaveney, M. J.: Regional relief characteristics and denudation pattern of the western Southern Alps, New Zealand, Geomorphology, 71, 402–423, https://doi.org/10.1016/j.geomorph.2005.04.013, 2005.

Leger, T. P. M., Jouvet, G., Kamleitner, S., Mey, J., Herman, F., Finley, B. D., Ivy-Ochs, S., Vieli, A., Henz, A., and Nussbaumer, S. U.: A data-consistent model of the last glaciation in the Alps achieved with physics-driven AI, Nat Commun, 16, 848, https://doi.org/10.1038/s41467-025-56168-3, 2025.

Levermann, A. and Winkelmann, R.: A simple equation for the melt elevation feedback of ice sheets, The Cryosphere, 10, 1799–1807, https://doi.org/10.5194/tc-10-1799-2016, 2016.

Liebl, M., Robl, J., Egholm, D. L., Prasicek, G., Stüwe, K., Gradwohl, G., and Hergarten, S.: Topographic signatures of progressive glacial landscape transformation, Earth Surf Processes Landf, 46, 1964–1980, https://doi.org/10.1002/esp.5139, 2021.

Meier, W. J.-H., Grießinger, J., Hochreuther, P., and Braun, M. H.: An Updated Multi-Temporal Glacier Inventory for the Patagonian Andes With Changes Between the Little Ice Age and 2016, Front. Earth Sci., 6, 62, https://doi.org/10.3389/feart.2018.00062, 2018.

Fiche climatologique. Statistiques 1981-2010 et records: https://donneespubliques.meteofrance.fr/FichesClim/FICHECLIM_73157002.pdf, last access: 28 November 2025.

Mey, J., Scherler, D., Wickert, A. D., Egholm, D. L., Tesauro, M., Schildgen, T. F., and Strecker, M. R.: Glacial isostatic uplift of the European Alps, Nat Commun, 7, 13382, https://doi.org/10.1038/ncomms13382, 2016.

Millan, R., Mouginot, J., Rabatel, A., and Morlighem, M.: Ice velocity and thickness of the world's glaciers, Nat. Geosci., 15, 124–129, https://doi.org/10.1038/s41561-021-00885-z, 2022.

Minh, N. Q., Huong, N. T. T., Khanh, P. Q., Hien, L. P., and Bui, D. T.: Impacts of Resampling and Downscaling Digital Elevation Model and Its Morphometric Factors: A Comparison of Hopfield Neural Network, Bilinear, Bicubic, and Kriging Interpolations, Remote Sensing, 16, 819, https://doi.org/10.3390/rs16050819, 2024.

Norris, S. L., Margold, M., Evans, D. J. A., Atkinson, N., and Froese, D. G.: Dynamical response of the southwestern Laurentide Ice Sheet to rapid Bølling–Allerød warming, The Cryosphere, 18, 1533–1559, https://doi.org/10.5194/tc-18-1533-2024, 2024.

Nowicki, S. M. J., Payne, A., Larour, E., Seroussi, H., Goelzer, H., Lipscomb, W., Gregory, J., Abe-Ouchi, A., and Shepherd, A.: Ice Sheet Model Intercomparison Project (ISMIP6) contribution to CMIP6, Geosci. Model Dev., 9, 4521–4545, https://doi.org/10.5194/gmd-9-4521-2016, 2016.

Patton, H., Hubbard, A., Andreassen, K., Auriac, A., Whitehouse, P. L., Stroeven, A. P., Shackleton, C., Winsborrow, M., Heyman, J., and Hall, A. M.: Deglaciation of the Eurasian ice sheet complex, Quaternary Science Reviews, 169, 148–172, https://doi.org/10.1016/j.quascirev.2017.05.019, 2017.

Pattyn, F., Perichon, L., Aschwanden, A., Breuer, B., de Smedt, B., Gagliardini, O., Gudmundsson, G. H., Hindmarsh, R. C. A., Hubbard, A., Johnson, J. V., Kleiner, T., Konovalov, Y., Martin, C., Payne, A. J., Pollard, D., and Price, S.: Benchmark experiments for higher-order and full-Stokes ice sheet models (ISMIP–HOM), The Cryosphere, 2008.

Penck, A. and Brückner, E.: Die Alpen im Eiszeitalter, Tauchnitz, 540 pp., 1909.

Rasmussen, S. O., Andersen, K. K., Svensson, A. M., Steffensen, J. P., Vinther, B. M., Clausen, H. B., Siggaard-Andersen, M. -L., Johnsen, S. J., Larsen, L. B., Dahl-Jensen, D., Bigler, M., Röthlisberger, R., Fischer, H., Goto-Azuma, K., Hansson, M. E., and Ruth, U.: A new Greenland ice core chronology for the last glacial termination, J. Geophys. Res., 111, 2005JD006079, https://doi.org/10.1029/2005JD006079, 2006.

Rückamp, M., Goelzer, H., and Humbert, A.: Sensitivity of Greenland ice sheet projections to spatial resolution in higher-order simulations: the Alfred Wegener Institute (AWI) contribution to ISMIP6 Greenland using the Ice-sheet and Sea-level System Model (ISSM), The Cryosphere, 14, 3309–3327, https://doi.org/10.5194/tc-14-3309-2020, 2020.

Rückamp, M., Kleiner, T., and Humbert, A.: Comparison of ice dynamics using full-Stokes and Blatter–Pattyn approximation: application to the Northeast Greenland Ice Stream, The Cryosphere, 16, 1675–1696, https://doi.org/10.5194/tc-16-1675-2022, 2022.

Schoof, C. and Hewitt, I.: Ice-Sheet Dynamics, Annu. Rev. Fluid Mech., 45, 217–239, https://doi.org/10.1146/annurev-fluid-011212-140632, 2013.

Seguinot, J., Ivy-Ochs, S., Jouvet, G., Huss, M., Funk, M., and Preusser, F.: Modelling last glacial cycle ice dynamics in the Alps, The Cryosphere, 12, 3265–3285, https://doi.org/10.5194/tc-12-3265-2018, 2018.

Strahler, A. N.: Quantitative analysis of watershed geomorphology, Eos Trans. AGU, 38, 913–920, https://doi.org/10.1029/TR038i006p00913, 1957.

Tadono, T., Ishida, H., Oda, F., Naito, S., Minakawa, K., and Iwamoto, H.: Precise Global DEM Generation by ALOS PRISM, ISPRS Ann. Photogramm. Remote Sens. Spatial Inf. Sci., II–4, 71–76, https://doi.org/10.5194/isprsannals-II-4-71-2014, 2014.

Valla, P. G., Shuster, D. L., and Van Der Beek, P. A.: Significant increase in relief of the European Alps during mid-Pleistocene glaciations, Nature Geosci, 4, 688–692, https://doi.org/10.1038/ngeo1242, 2011.

Whitbread, K., Jansen, J., Bishop, P., and Attal, M.: Substrate, sediment, and slope controls on bedrock channel geometry in postglacial streams, JGR Earth Surface, 120, 779–798, https://doi.org/10.1002/2014JF003295, 2015.

Wickert, A. D.: Open-source modular solutions for flexural isostasy: gFlex v1.0, https://doi.org/10.5194/gmdd-8-4245-2015, 2 June 2015.

Williams, C. R., Thodoroff, P., Arthern, R. J., Byrne, J., Hosking, J. S., Kaiser, M., Lawrence, N. D., and Kazlauskaite, I.: Calculations of extreme sea level rise scenarios are strongly dependent on ice sheet model resolution, Commun Earth Environ, 6, 60, https://doi.org/10.1038/s43247-025-02010-z, 2025.

Winkelmann, R., Martin, M. A., Haseloff, M., Albrecht, T., Bueler, E., Khroulev, C., and Levermann, A.: The Potsdam Parallel Ice Sheet Model (PISM-PIK) – Part 1: Model description, The Cryosphere, 5, 715–726, https://doi.org/10.5194/tc-5-715-2011, 2011.

Wirsig, C., Zasadni, J., Christl, M., Akçar, N., and Ivy-Ochs, S.: Dating the onset of LGM ice surface lowering in the High Alps, Quaternary Science Reviews, 143, 37–50, https://doi.org/10.1016/j.quascirev.2016.05.001, 2016.

Yan, Z., Leng, W., Wang, Y., Xiao, C., and Zhang, T.: A comparison between three-dimensional, transient, thermomechanically coupled first-order and Stokes ice flow models, Journal of Glaciology, 69, 513–524, https://doi.org/10.1017/jog.2022.77, 2023.

Zhang, R., Zhang, Z., Jiang, D., Ramstein, G., Dupont-Nivet, G., and Li, X.: Tibetan Plateau Made Central Asian Drylands Move Northward, Concentrate in Narrow Latitudinal Bands, and Increase in Intensity During the Cenozoic, Geophysical Research Letters, 49, e2021GL093718, https://doi.org/10.1029/2021GL093718, 2022.